Coastal Oceanography Applications of Digital Image Data from Marine Radar

I. S. ROBINSON, N. P. WARD, C. P. GOMMENGINGER, AND M. A. TENORIO-GONZALES

Department of Oceanography, Southampton Oceanography Centre, University of Southampton, Southampton, United Kingdom

(Manuscript received 11 May 1998, in final form 28 June 1999)

ABSTRACT

A marine radar attached to a digital image capture system has been adapted for deployment from shore sites. Optimum operating parameters have been identified in relation to the resolution and sampling capabilities of both the radar and the digitization system. Special software enables individual images to be geographically located so that several images can be averaged to reduce speckle and to eliminate features that fluctuate at high frequency. Test deployments at several coastal sites in the south of England confirm that the system is capable of making unique measurements for a variety of oceanographic applications in the coastal zone. The spatial distribution of wave crests approaching the shore can be measured, and by averaging over time, the location of the breaker zone can be established. Although the precise mechanisms for backscatter of grazing incidence radar are not fully understood, it is clear that the radar can also detect the surface signatures of estuarine fronts and wastewater discharge plumes. The interaction between tidal flow and bathymetric features can also be detected by the surface roughness signature. The radar is particularly useful for monitoring the gradual evolution of processes over a tidal cycle.

1. Introduction

In recent years, oceanographers have discovered a variety of scientific applications for imaging, oblique-viewing radars on aircraft and satellites, following the development of high-resolution synthetic aperture radars (SARs) operating at a variety of frequencies. In contrast, conventional X-band, grazing incidence, marine radar systems, which are a mature technology widely used on ships for navigation, have only occasionally been employed for scientific purposes. Most recent improvements in the display processing for marine radars have been primarily concerned with eliminating the contribution of radar backscatter from the ocean, which is referred to as sea clutter and is rarely considered as a potential source of oceanographic information. There is no justification for this apparent neglect of marine radars by oceanographers. This paper presents the results of recent experiments that demonstrate the effectiveness for a number of scientific applications of marine radars based at coastal sites. Given simple modifications to capture digital image signals, the marine radar can be transformed into a quantitative instrument of considerable utility for coastal oceanographers, which offers sampling capabilities to complement those of airborne and satellite radars.

Grazing incidence radars have been built and used for research purposes, leading to a broad understanding of the physics of sea clutter, which underpins the interpretation of image data captured from marine radars (Wetzel 1990). Of particular concern has been the discrepancy between the magnitude of horizontally polarized radar echoes (see, e.g., Trizna 1991) and the much smaller predictions of standard composite radar scattering models. It is now the consensus from laboratory studies that a significant contribution to horizontally polarized grazing incidence radar backscatter comes from breaking wave events at a variety of scales, generating so-called sea spike echoes (Trizna et al. 1991). Trizna and Carlson (1996) have demonstrated this also in the coastal zone.

Previous oceanographic uses of marine radar have normally worked with the standard display of navigation radars on research vessels (Williams 1978). Kerry et al. (1984) used images from ships' radars in the detection of the surface roughness signatures of internal waves. Marine radars have also been used to observe oil slicks on the sea surface (DeLoor et al. 1986; Tennyson 1988). Marine radars based on shore are used by coast guard services in monitoring shipping traffic, and these too have been used for oceanographic purposes. Watson and Robinson (1990) obtained a sequence of photographic records from a radar based at Gibraltar in order to examine the propagation of internal waves through the Strait of Gibraltar. They were limited by the cumber-

Corresponding author address: Dr. Ian S. Robinson, Department of Oceanography, Southampton Oceanography Centre, University of Southampton, European Way, Southampton SO14 3ZH, United Kingdom.
E-mail: ian.s.robinson@soc.sobn.ac.uk

FIG. 1. Photograph of marine radar deployed from a van at a coastal location.

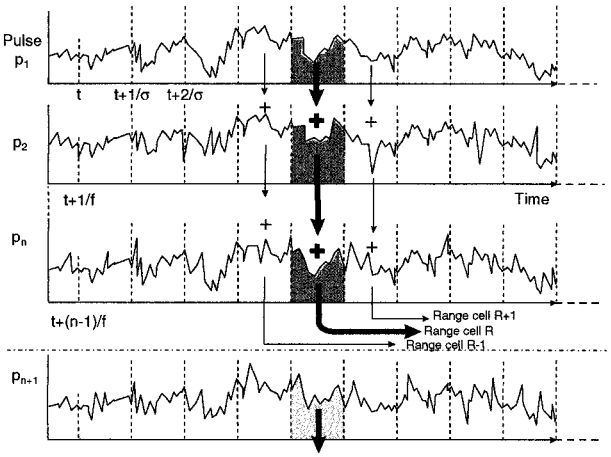

FIG. 2. Signal capture sequence by a Wavex board.

some technology of digitizing photographic records in order to recover information about the movement of features from one image to another. They also noted that if the display parameters are optimized to reveal patterns of sea clutter in one part of the image, the patterns are lost from other parts. It would be far more satisfactory to digitize the radar signal directly before it is used to construct the conventional black and white (1 bit) or black, white and two gray tones (2 bit) image displays in which most of the information about the magnitude of the backscattered signal has been lost. Radiometric resolution at an 8-bit digitization or better would permit far more information to be collected, and digital signal processing should further enable perturbations to be distinguished from mean and baseline patterns of radar return.

The technology to achieve digital capture of the return signal received by a marine radar is now available. Systems have been developed with the objective of measuring two-dimensional wave spectra at sea (Hirakuchi and Ikeno 1990). Results from this approach are now appearing in the literature (Buckley et al. 1994; Trask et al. 1994; Seemann et al. 1997); but present use seems to be limited mainly to observing wave spectra.

In this paper we describe how a marine radar system with digital capture has been developed expressly for deployment from coastal sites overlooking inshore waters. In the next section the instrument, its capabilities, and mode of deployment are described. This is followed by an analysis of the system's spatial and temporal sampling capabilities, and a description of the processing software that generates images corresponding to maps of the ocean microwave backscatter distribution in geographical coordinates. Several case studies are then presented to illustrate the effectiveness of the radar to detect the refraction patterns of waves approaching a coast, the location of the surface signature of coastal discharge from rivers and from sewage outfalls, the position of breaker zones on an exposed beach, and the location of a submerged sandbank. The paper also examines three cases in which a time sequence of images yields unique information about the dynamic evolution of a coastal front, the tidal movement of the discharge from an outfall pipe, and the propagation dynamics of waves approaching a beach.

2. Digital capture of marine radar data

The radar system used in this work is a Racal Decca model 1070A, which would normally be used as a ship's navigation radar. Signals from the radar are fed to a Wavex digital capture board installed in a DOS-based

TABLE 1. Variables for the radar and digital capture system.

	System variable	Symbol	Parameter range	Effect on image
Radar settings	Pulse repetition frequency (PRF)	f	600 1200, 2400 Hz	Azimuth sampling interval
	Pulse length	τ	0.08–1 μs	Range resolution
	Antenna beamwidth	β	Fixed, 1°	Azimuth resolution
	Antenna rotation period	T	Fixed, 2.4 s	
Capture board settings	Azimuth start angle	θ	0°–360°	Size and location of image
	Azimuth interval	ϕ	0°–360°	Size and location of image
	Initial delay	d	0.6–25.4 μs	Size and location of image
	Burst duration	D	0.2–51 μs	Size and location of image
	Sampling rate	σ	5, 10, 20 MHz	Range resolution
	Azimuth step	n	1–16 pulses	Azimuth resolution
	No. of repeat images	N	1–256	

TABLE 2. Definition of cell size and resolution.

Cell size in azimuth angle	$\frac{\text{rotation rate} \times \text{azimuth step size}}{\text{pulse repetition rate}}$,	$\frac{360n}{Tf}$
Cell size in range	$\frac{\text{speed of light}}{2 \times \text{sampling frequency}}$,	$\frac{c}{2\sigma}$
Azimuth resolution	angular beam width,	β
Range resolution	$\frac{\text{pulse length} \times \text{speed of light}}{2}$,	$\tau c/2$

personal computer, which is capable of sampling up to 20 MHz. For coastal deployments the radar system has normally been installed in a van or minibus as shown in Fig. 1. For this type of radar the rotating antenna is attached directly to the radar scanner containing the microwave generator (magnetron), and this is mounted on the roof of the van during deployment. Inside the vehicle, the operating personnel are protected from irradiation by the emitted microwaves. The computer is installed inside the vehicle and the whole system is powered electrically by a portable generator. The radar system is therefore entirely autonomous and can be set up rapidly at a wide variety of coastal sites.

Three outputs from the radar are fed to the Wavex board. The first is a heading marker, which signals once each revolution of the antenna. Since the system is stationary when in use, this occurs when the antenna is pointing in a particular direction determined by the orientation of the radar system and the vehicle. The second output is a trigger pulse produced each time a microwave burst is emitted. For a known pulse repetition rate, counting this provides an estimate of the angular position of the antenna relative to the heading marker. Finally, the video line carries the demodulated and logarithmically compressed signal from the receiver section of the radar. This is the signal that is sampled at high frequency, digitized, and stored by the Wavex board.

The Wavex board operates by sampling the time history of the return signal from a single pulse, which is digitized within each of 512 discrete segments. This may be repeated, integrating the signal from corresponding segments of several pulses, then storing the resulting numbers before emptying the registers to start integrating from the next pulse (see Fig. 2). Onboard digitization is performed with 16-bit resolution, and the data are subsequently reduced to 8 bits for storage. Integration of adjacent pulses by simple averaging could lead to problems with calibration since the signal is the output of a logarithmic amplifier. Ideally, averaging should be performed only after applying the receiver transfer function, but this is not possible with the given hardware. This must not be ignored in applications in which calibration of the data is attempted.

By adjusting various radar and data capture settings, the sampling capabilities of the system can be matched to the phenomenon under study. The variables are listed in Table 1. The radar pulse repetition frequency (PRF) has a fundamental effect on the rest of the setting options. Primarily it affects the azimuth sampling rate (or azimuth step), but, by putting a constraint on how long the return signal can be monitored before the next pulse, it also affects the range of the radar. In addition it determines the logarithmic amplification and the level of emitted power.

It is important when defining the imaging capabilities of the system to distinguish between the dimensions of the sampling cells and the inherent resolution of the

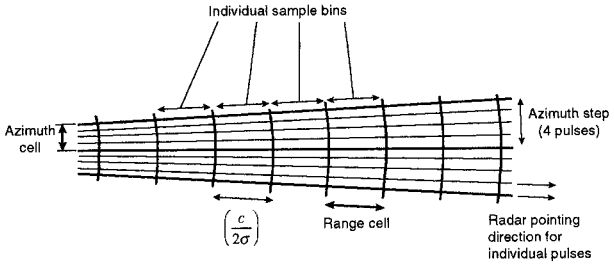

FIG. 3. Azimuth and range cell definition.

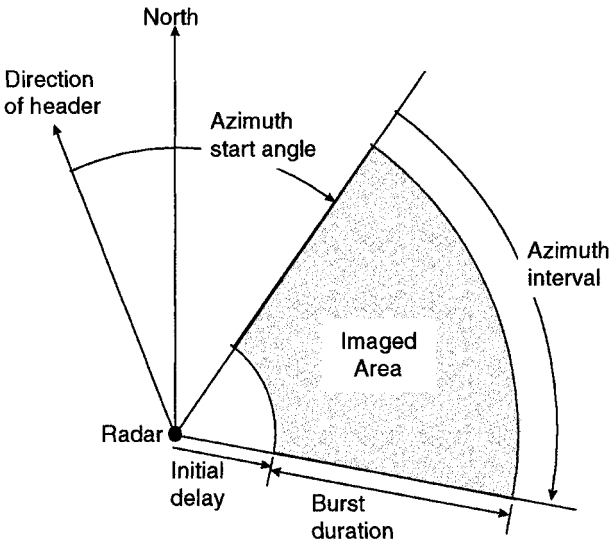

FIG. 4. Definition of captured image area.

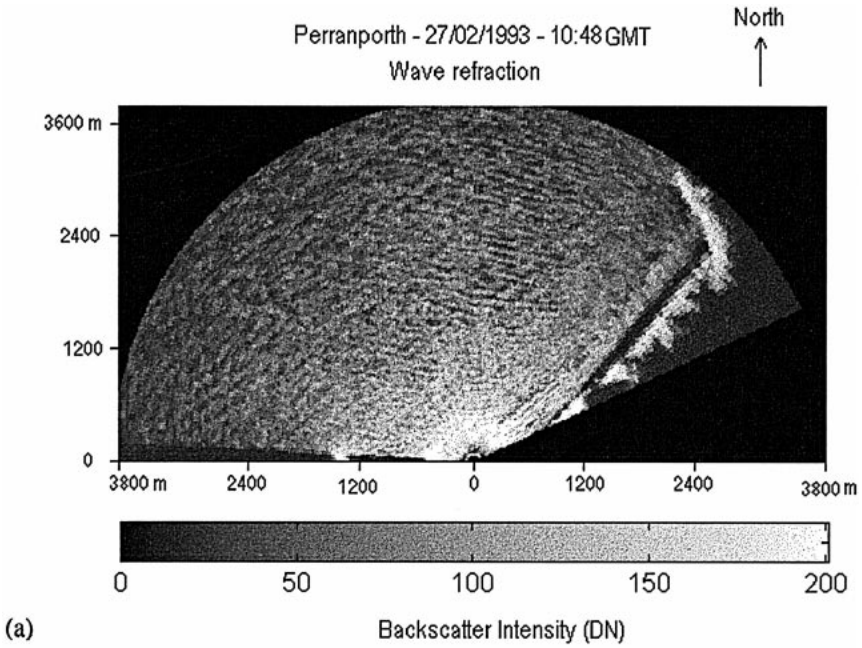

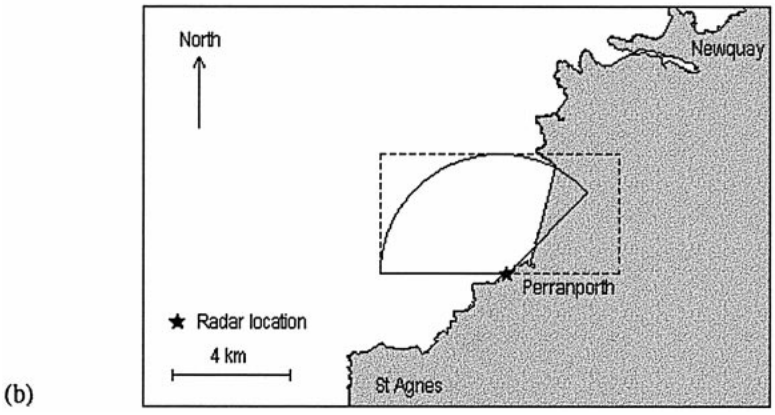

FIG. 5. (a) A single captured short-pulse radar image of swell waves approaching Perranporth beach, 1048 UTC 27 Feb 1993. The digital number (DN) is proportinal to backscatter echo intensity. (b) Location map, and (c) 2D FFT of the central part of the image.

radar, as defined in Table 2. The range size of the sampling cells for the digitized data is determined by the sampling rate selected for the Wavex board operation. This is illustrated in Fig. 3, which also shows how the azimuth angular width of the cells is controlled by the PRF and the azimuth step size. The 5-, 10-, or 20-MHz Wavex sampling rates lead to range cells of, respectively, 30, 15, or 7.5 m. The inherent resolution determines the smallest size of a feature that can be distinguished on the sea surface. For efficient operation it is desirable to match the resolution and the sampling cell size. The radar pulse length sets the limit on how fine the range resolution can be, while the azimuth resolution depends on the radar antenna's beamwidth. The shortest pulse length available from this radar is 0.08 μs, giving a pulse-averaged range length of 12 m at the sea surface. This sets a limit to the effective range resolution. Such a short pulse limits the output power and thus the maximum range of the radar to 3–4 km. For larger ranges, a longer pulse with higher output power must be used, with consequently poorer range resolution.

The geographical location and extent of the region, which is imaged by the system, is controlled by further capture board settings (see Fig. 4). The azimuth start angle and azimuth interval determine how wide an angle of view is captured, and where it is located relative to the heading direction. The initial delay defines the closest range that is captured, and the burst duration defines

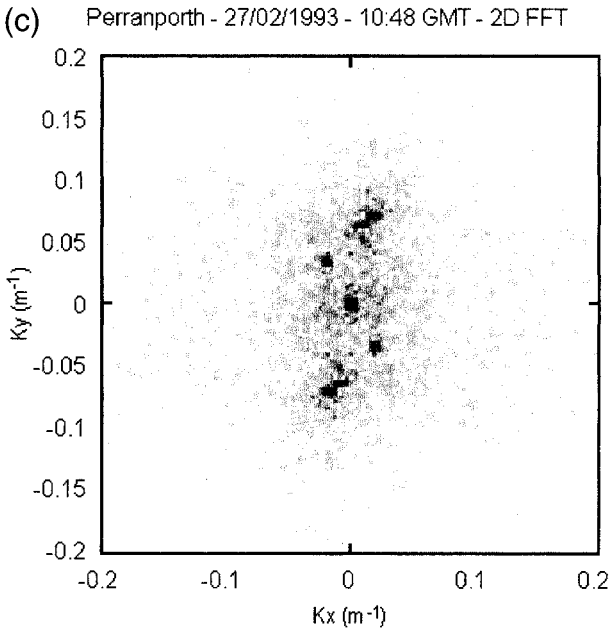

FIG. 5. (c) (*Continued*)

the range width. Permitted settings for these parameters are constrained both by the radar parameters (e.g., the burst duration plus the initial delay must be shorter than the time between pulses) and by the board capacity (the burst duration cannot be more than the sampling interval times the maximum number of samples).

The number of images that can be captured in one sequence is limited by the Wavex software to 256 images. In theory, the interval between successive images is determined by the antenna rotation rate (25 rpm). In practice, however, the Wavex can capture separate images from successive rotations only if the radar is set for short-range use at the maximum PRF. Typical settings, which maximize the resolution and optimize the sampling cell size for the inherent resolution, are listed in Table 3.

3. Data processing

The data are stored as records consisting of radar backscatter from a series of ranges at each specific azimuth angle. These can be displayed as *x, y* plots of range and azimuth in order rapidly to check the system behavior. The object of subsequent data processing is to produce a digital image that corresponds to the magnitude of energy backscattered from different parts of the sea surface at a given time corresponding to a particular antenna rotation. Resampling into a rectangular format is necessary to facilitate subsequent geometric adjustment, geographical location, and comparison with other data. The reconstruction of a Cartesian coordinate image from the radial data is performed by placing each data point into its mapped output pixel and then averaging all such contributions to a pixel.

The choice of output pixel size is influenced both by the range and azimuth cell sizes and also by the radial geometry. The normal compromise is to select radar and Wavex settings that result in the linear cell dimension in the azimuth being about equal to the range cell size at the center of the image. Both of these should be similar to the resolution. The square Cartesian cell is then chosen to have sides equal to the range cell size. For pixels mapped from the near range, there is azimuthal oversampling, whereas at far range the pixels are undersampled in the azimuth. If necessary, unfilled pixels at the far range have to be filled by their nearest neighbor. The possibility of image degradation at large range must be remembered when images are being analyzed.

A suite of image processing software has been written to perform a variety of operations on the image data (see Table 4). These procedures have been written with careful attention to the radial nature of the original data and are preferred to simply applying proprietary image processing software to the resampled Cartesian image. For example, the geometric correction operates from the original data captured from azimuthal beams rather than the resampled Cartesian image data.

The averaging function is an important one that enables the benefits of digital capture to be readily exploited. Given the nature of radar and the fluctuations in the ocean surface profile, individual images are often noisy. A certain amount of oversampling in the digital capture process (especially at near range) helps to reduce this. Averaging over several images, provided they overlay geographically, enables any permanent underlying

TABLE 3. Typical radar and data capture settings.

	High-resolution images	Intermediate scale	Wide area coverage
Radar PRF	2400 Hz	1200 Hz	600 Hz
Radar pulse length	0.08 μs	0.3 μs	1 μs
Sampling rate	20 MHz	10 MHz	5 MHz
Azimuth steps	16	8	4
Range resolution	12 m	45 m	150 m
Azimuth resolution	1°	1°	1°
Range cell size	7.5 m	15 m	30 m
Azimuth cell size	1°	1°	1°
Burst duration	12.5–25.5 μs	25.5–51 μs	51 μs
Maximum image range	2–4 km	4–8 km	8 km

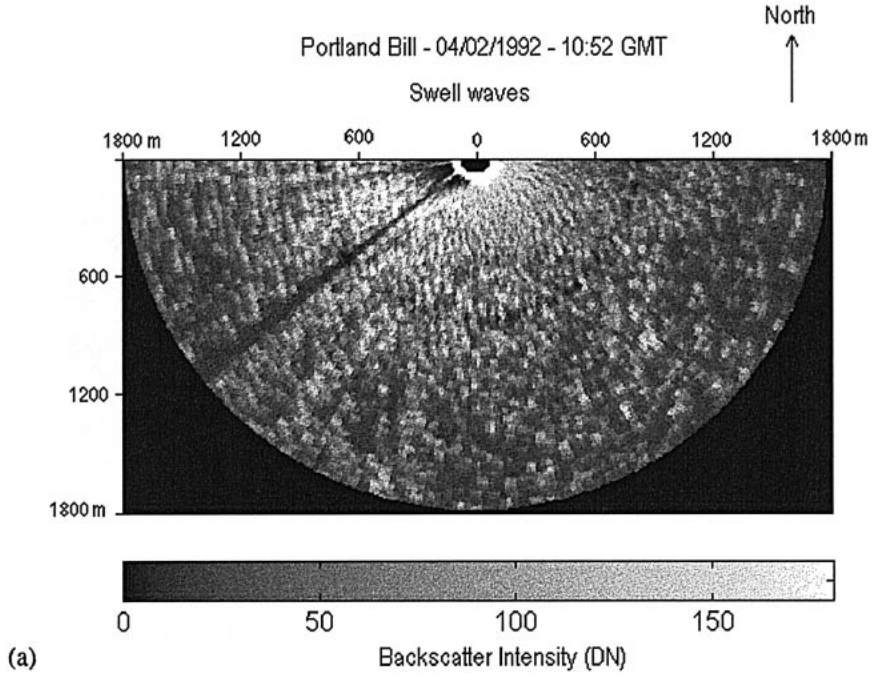

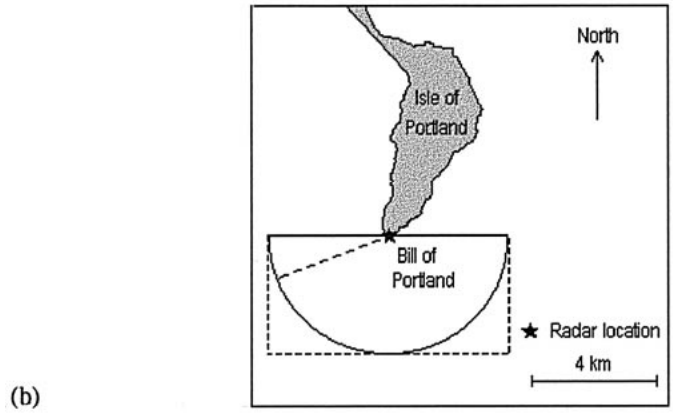

FIG. 6. (a) A single captured short-pulse radar image of swell waves passing Portland Bill, 1052 UTC 4 Feb 1992. The dark radial lines are artifacts caused by objects close to the radar site that block the radar transmission over a small range of azimuth angles. (b) Location map.

features that affect the backscatter to be strongly enhanced, as will be demonstrated below.

Recent work has developed algorithms for the normalization of the radar images into maps of the ocean Normalized Radar Cross Section (NRCS). The object is to recover an image corresponding to the grazing NRCS of each pixel area of the sea, independent of how close it was located to the radar and the power output used for the data capture. A detailed description of this procedure in the context of accurate calibration of the system is presented by Gommenginger et al. (2000). Here we will demonstrate the utility of uncalibrated image data for observing a variety of coastal ocean phenomena. Examples of how the additionnal quantitative information produced from NRCS images can be exploited for oceanographic purposes is left for a later publication.

4. Observation of rapidly changing phenomena

In order to investigate the utility of the digital radar capture system for coastal marine science, it has been deployed at a number of locations on the English south

TABLE 4. Image processing operations.

Operation	What it accomplishes
Image	Resamples the radial data into a Cartesian image with square pixels.
Histogram	Generates a histogram of the values of pixels in the image.
Geometric correction	Ground control points of known location, identified in the image, are used to geolocate all pixels and resample to map projection.
Filters	3×3 smoothing filters can be applied.
Average	Averages the sequential images from a series of captured data.
1D FFT	Evaluates the Fourier spectrum of the spatial variation along a transect through the image.
Transect	Plots the data values along a linear transect through the image.
2D FFT	Evaluates the 2D spatial Fourier spectrum of part of the image.

coast, in some instances coupled with other coastal oceanography experiments.

The first examples are of swell waves in coastal regions. Figure 5 illustrates a single image obtained from a deployment off the southwest coast of England. It clearly shows waves with a characteristic wavelength of 95 m from the north-northeast being refracted as they approach the beach. In addition, there is another family of 150-m waves approaching from the northwest. The two different wave trains are revealed clearly on the 2D fast Fourier transform (FFT) (Fig. 5c) from which their wavelengths and directions can be confirmed. This image demonstrates that the radar is able to image waves traveling in a variety of orientations including both the range and azimuth directions.

Another example of the imaging of coastal waves, shown in Fig. 6, has been obtained at Portland, a prominent headland in the English Channel. In this case the waves are propagating past the headland (from left to right in the figure) and exhibit some refraction and possibly diffraction to the south and east of the headland (close to the radar site in the image). Once again, the radar appears to be capable of imaging both range and azimuth traveling waves. The dark shadow on the image, from the radar toward the southwest, is an artifact resulting from the shadow cast by a post close to the instrument on the cliff top.

In both these cases, the phenomenon must be observed on individual images only because the timescale for change is of the order of a few seconds. Averaging two consecutive image datasets captured 2.4 s apart would cancel rather than reinforce the wave patterns. In the far field of both images the waves become less distinct, especially those traveling in the azimuth direction, because of the coarser spatial resolution in the azimuth direction at a large range. Both of these deployments used short pulses to improve the range resolution and enable the detection of wavelengths of about 100 m.

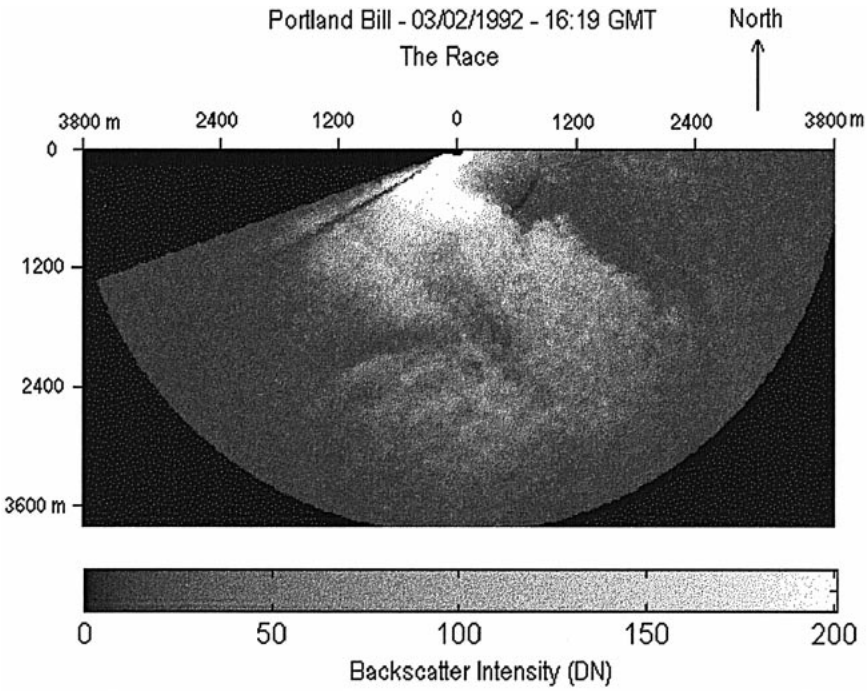

FIG. 7. Average of eight captured medium pulse radar images off Portland Bill, 1619 UTC 3 Feb 1992. Note the relatively dark and bright features, especially in the right-hand portion of the image, that are thought to be due to wave–current interaction.

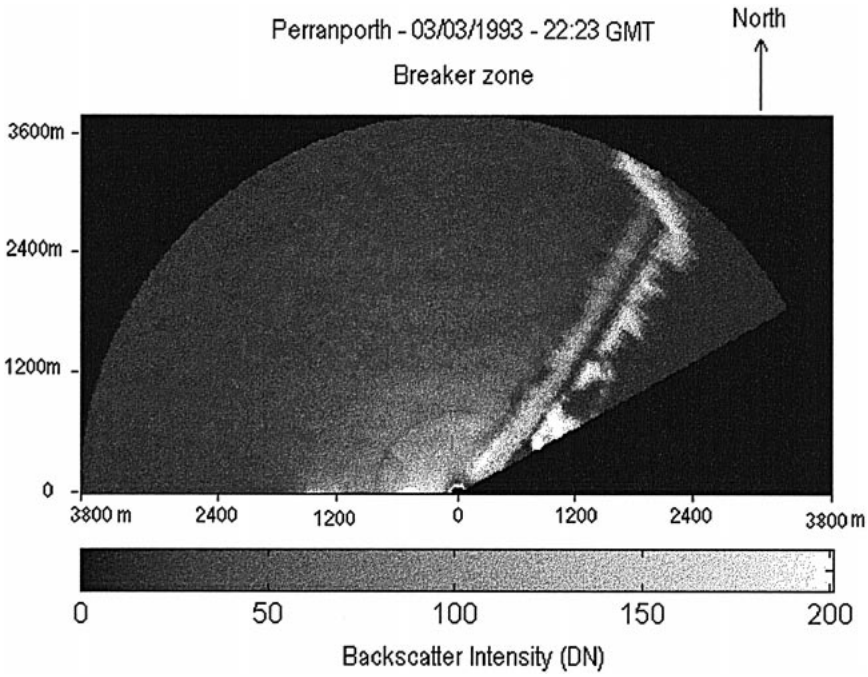

FIG. 8. Average of eight captured short pulse radar images in Perranporth Bay, 3 Mar 1993.

The Perranporth deployment was from a relatively high cliff, thus increasing the elevation angle and strengthening the radar return from the farthest range, whereas the Portland deployment was only a few meters above sea level, with a consequent reduction in maximum detectable backscatter range.

The question of why the swell waves should appear at all on the radar image is not readily answered. Evidently there is modulation of the backscattered microwave energy, which is phase-coupled to the surface swell. The mechanisms by which oblique-viewing radars can record images of surface waves have been examined in considerable detail (e.g., Wright 1968; Valenzuela 1978), but the imaging mechanisms for grazing radars are less well understood (see, e.g., Chan 1990 and Malinovsky 1992). The Bragg interaction mechanism causes the radar backscatter to be sensitive to the short surface waves whose length is half that of the microwaves. The hydrodynamic modulation of the short surface waves by the long waves would therefore lead to the long waves being imaged. Furthermore, tilting by the large-scale waves of local surface facets much larger than the radar wavelength is important since the scattering is sensitive to changes in incidence angle. However, at grazing incidence other factors affect the backscatter, such as the shadowing of part of the sea surface by the crests of longer waves. Another possibility is that steep or breaking short waves may present localized facets having much smaller radar incidence angles and hence higher backscatter, or may even cause specular reflections. The current preferred hypothesis on microwave backscatter at grazing incidence is that wedge scattering (Lee et al. 1995), sea spikes (Trizna 1991; Trizna et al. 1991), and multipath effects (West et al. 1996) provide significant contributions to the ocean backscatter, especially at horizontal polarization (as in the system presented here). Although these are important questions requiring further study, the emphasis in this paper is to adopt an empirical approach regarding the capability of the radar system to observe ocean phenomena. We shall consider the matter further in the light of some of the other phenomena that the radar records, but leave to future papers a fuller investigation of imaging and backscatter mechanisms.

5. Identification of stationary oceanographic features

In further experiments we have identified a number of situations where, by averaging over a number of images collected in rapid succession, quasi-stationary oceanographic features can be detected behind the rapidly varying high-frequency sea clutter and ocean wave signal.

a. Portland tide race

Figure 7 shows an image covering a similar area to Fig. 6, but averaged over eight rotations of the radar (about 20 s—at least two wave periods). While the individual waves can no longer be detected, it is now possible to observe the underlying distribution of backscattered microwave energy, probably corresponding to the distribution of mean surface roughness. Ignoring the

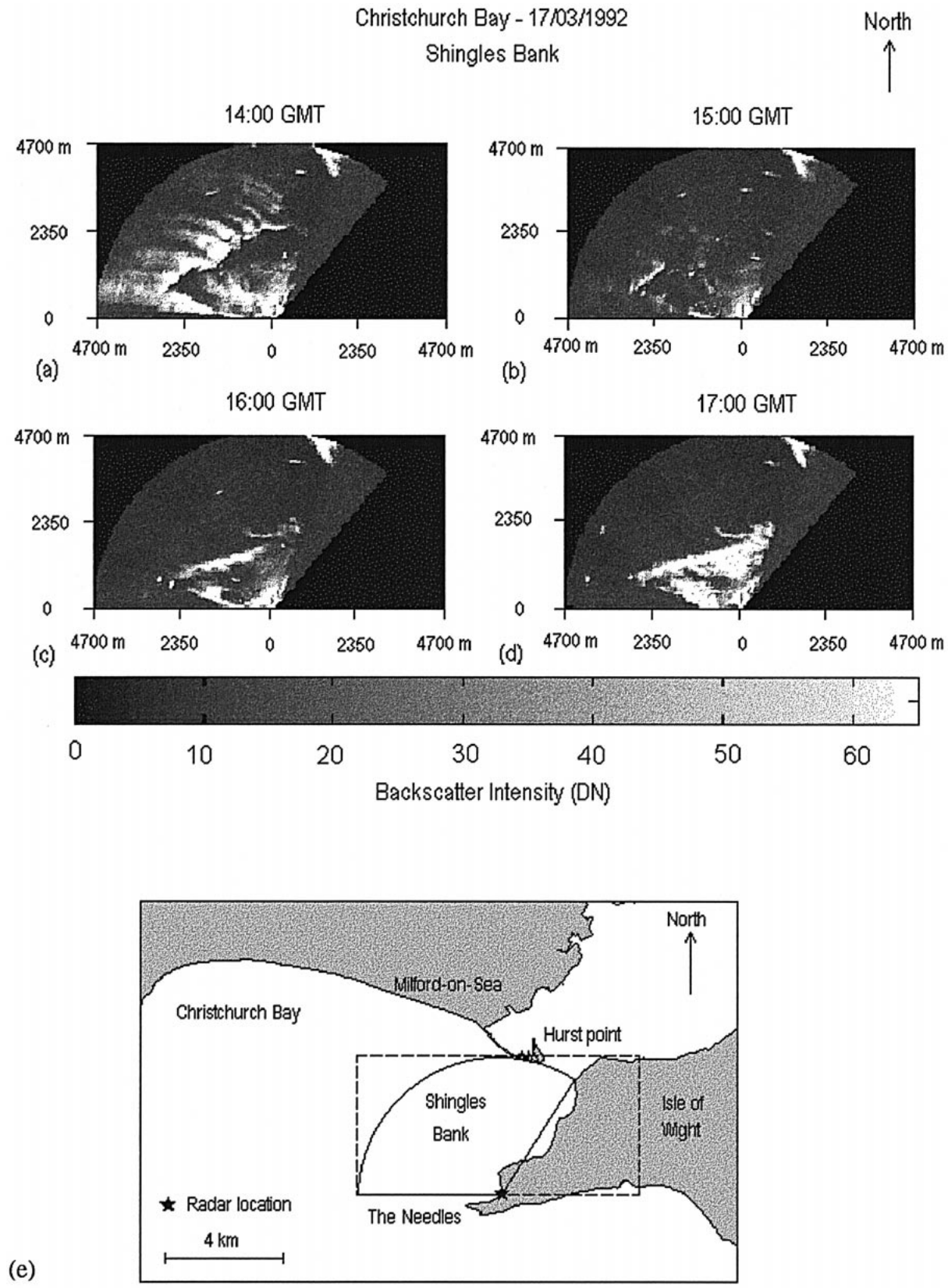

FIG. 9. Sequence of eight-capture averaged medium pulse radar images over the Shingles Bank, 17 Mar 1992 at (a) 1400, (b) 1500, (c) 1600, and (d) 1700 UTC. (e) Location map.

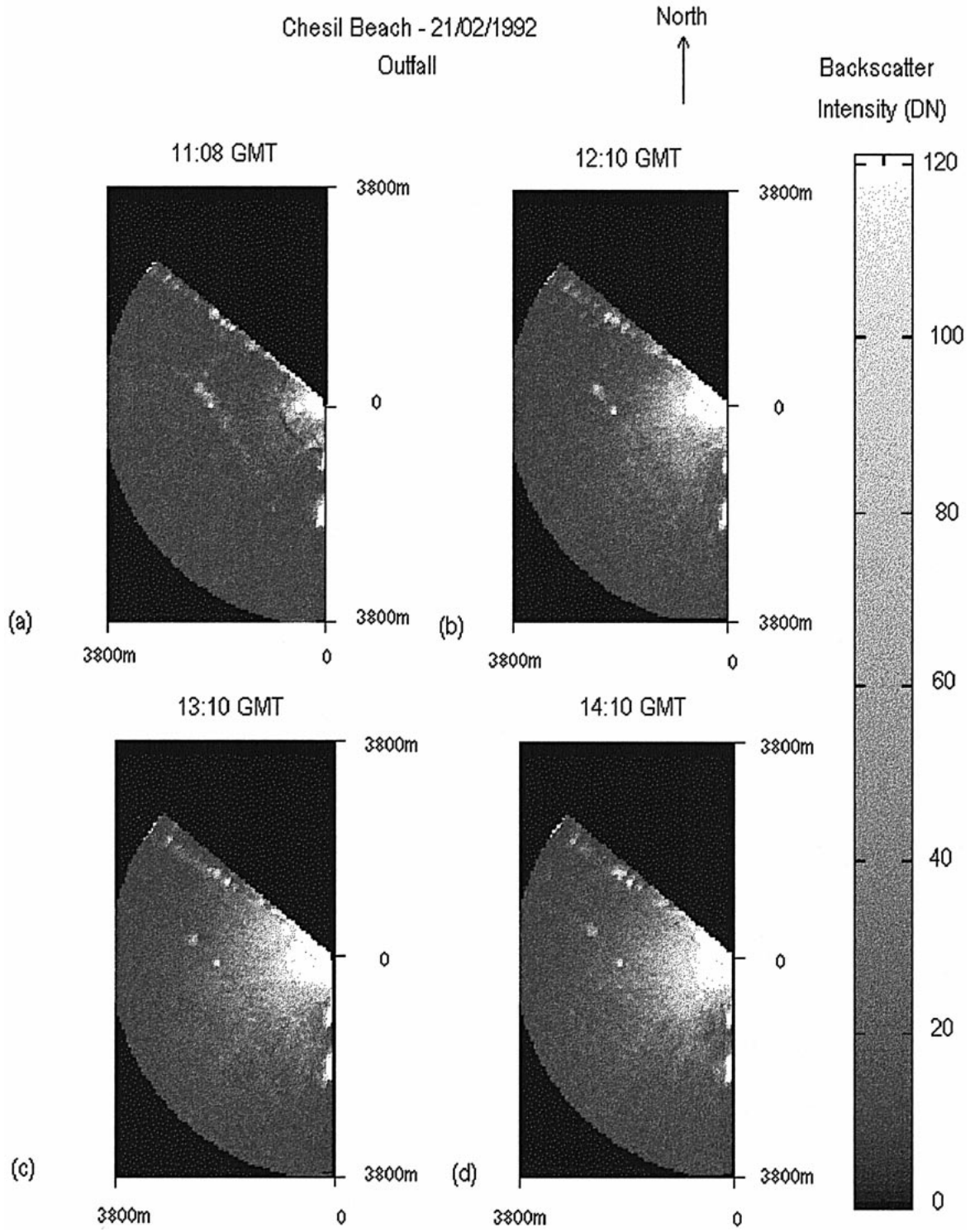

FIG. 10. Sequence of eight-capture averaged medium pulse radar images off Chesil Beach on 21 Feb 1992 at (a) 1108, (b) 1210, (c) 1310, and (d) 1410 UTC. (e) Location map.

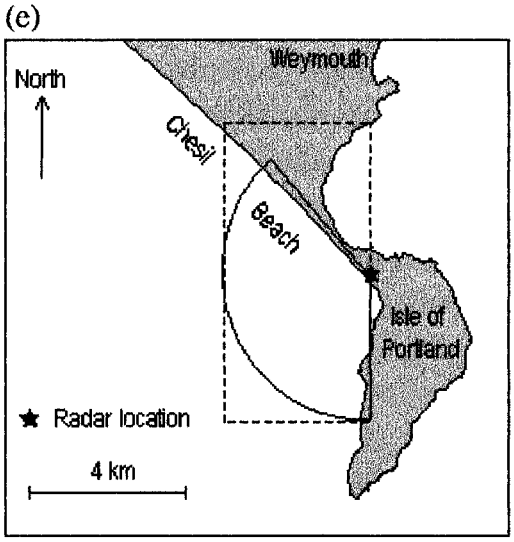

FIG. 10. (e) (*Continued*)

shadow and the low amplitude circle at about 900-m range, which are radar artifacts, and allowing for some range dependency of the return signal strength, there remains an interesting spatial distribution of surface roughness. Southwest of the radar and within 1 km of the coast the backscatter is strongest, and farther offshore there are distinct steps in apparent roughness. The most evident of these is southeast of the radar. The most probable explanation for this is that wave–current interaction is occurring with the strong tides that flow past the headland over a number of ledges and troughs in the bathymetry. Eight-revolution averaged images acquired at other states of the tide show similar patterns but in different places that shift gradually, reinforcing the conclusion that the patterns are tidally controlled although there may be an influence from the wind. It is not clear whether it is the inhomogeneity of the amplitude of the longer waves, such as those imaged in Fig. 6, or the energy of the shorter gravity waves contributing to the general sea clutter, or both, which give rise to the patterns of higher and lower backscatter. This phenomenon is being studied further.

b. Perranporth breaker zones

Figure 8 demonstrates the benefit of averaging images of a beach zone over a number of wave periods. It comes from Perranporth Bay, on the northwest facing coast of Cornwall in England, but on a different day than the images in Fig. 5, when the beach was exposed to quite strong swell from the Celtic Sea. The image identifies where, on average, the surface is roughest. There is a well-defined breaker zone, separated from the highly reflective coastline and cliffs by a clearly distinguished zone of low backscatter. Some variation of the width of the breaker zone and its distance from the shore is evident along the 3-km beach. The radar is capable of recording low-frequency fluctuations of the breaker zone over minutes, and its movement on- and offshore with the tide. The simplicity with which this information can be derived from a single instrument contrasts with the difficulty of conventional techniques used to monitor beach processes.

c. Shingles Bank

The ability of synthetic aperture radars to map the location of shallow seabed topography has been amply demonstrated by a number of satellite-borne sensors (e.g., Alpers and Hennings 1984). Tidal flow over undulating seabed topography results in spatially fluctuating currents, which modulate the short surface waves that govern microwave scattering. This phenomenon is well known to mariners who can detect shallow banks in coastal waters by their surface signature. Such fluctuations are generally too weak, in comparison with the variability caused by long surface waves and by random speckle, to be evident on radar screens in real time. However, once the high-frequency fluctuations have been removed by averaging over a number of sequential images, the gradual changes in backscatter related to the underlying topography should be detectable in suitable tidal conditions.

Figure 9 confirms this idea. The Shingles Bank, off the entrance to the West Solent, is clearly defined in this sequence of four hourly spaced images. The bank is revealed at 1400 UTC by the region of enhanced backscatter to left of center of the image. Note the sharp edge of the bright zone corresponding to the crest of the bank. At this time the tide was flowing southwestward into the English Channel from the West Solent. One hour later, at slack water, the radar signature of the bank has disappeared. In the subsequent two hours, as the tidal stream starts to flow to the northeast, the radar signature reappears but now in reverse, with low backscatter to the northwest of the crest and high backscatter to the southeast, with a sharp edge close to the crest line. Further study is required to determine whether the marine radar, averaging over several rotations, is integrating the effect of breaking waves, increased amplitude of the regular swell, or enhancement of the short-scale locally generated wind waves, to produce the topographically related patterns of backscatter.

Each of the images in Fig. 9 is comparable in its bathymetric information content with satellite images from the *ERS-1* SAR, which covers the same area (Scoon and Robinson 1993). The advantage of the coastally sited marine radar is that it can monitor the phenomenon throughout a single tidal cycle, which is not possible with satellite SARs. The radar should have the capability to detect movement and changes in the seabed features if deployments are repeated under similar tidal conditions from the same location over several years.

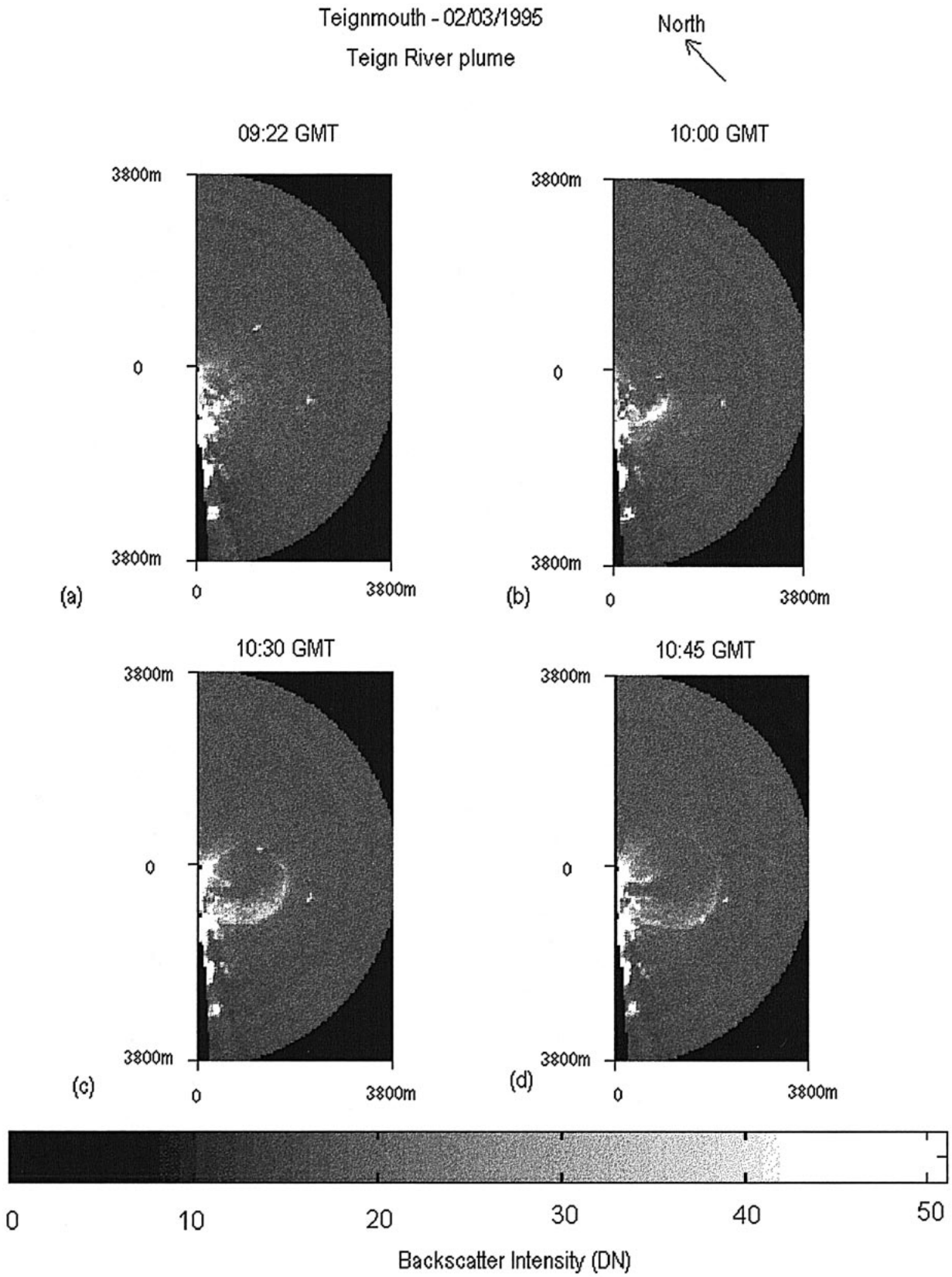

FIG. 11. Sequence of eight-capture averaged short pulse radar images off Teignmouth on 2 Mar 1995 at (a) 0922, (b) 1000, (c) 1030, and (d) 1045 UTC. (e) Location map.

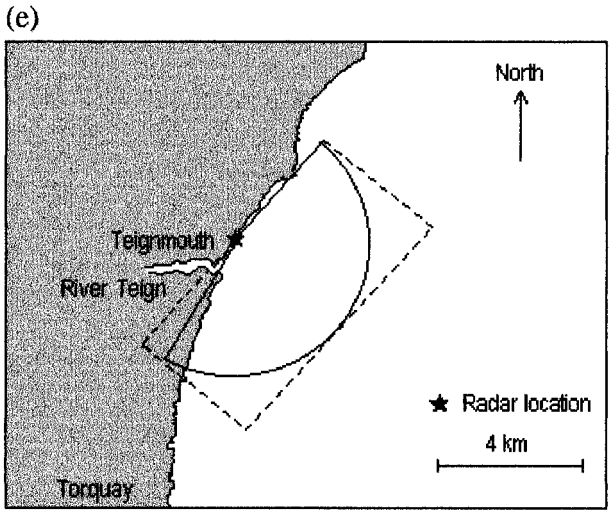

FIG. 11. (e) (*Continued*)

6. Detection of slowly moving features

a. Outfall at Chesil

One particularly useful feature of the marine radar in comparison with other imaging radar methods from aircraft and satellites derives from its stationary location and the relative ease with which repeat sampling of the same image area can be undertaken. Its potential lies not only in the capacity to average out high-frequency fluctuations over several minutes, as demonstrated in the previous section, but also in the possibility of being able to repeat those averages regularly over a longer period. In this way the evolution of features can be monitored throughout the tidal cycle, during the passage of a weather front or for the duration of any other phenomenon, which may cause environmental conditions to change gradually in coastal waters. It can thus provide the time varying context in which to interpret single ''snapshot'' satellite radar images.

This is well illustrated in Fig. 10 by the serendipitous observation of the surface signature of a piped discharge. The bright spot on all the images due west of the radar is a reflecting buoy. In Fig. 10a there is a plume of enhanced backscatter stretching from the buoy to the northwest. The persistence of this feature over several independent capture sequences confirmed it as a real and quasi-permanent phenomenon. The only clue to its origin comes from the local hydrographic chart, which records the existence of a seabed piped discharge at approximately the same place. We suggest the hypothesis that flow discharging from the pipe reaches the surface and in some way alters the roughness detected by the radar. Normally a discharge plume might be expected to contain surfactant material and thus produce a surface slick, resulting in smoother sea surface conditions and consequently reduced backscatter and a dark signature on the radar image. However, the bright patch implies increased backscatter and a rougher surface. There was no visual evidence of anything causing the roughness, and it was difficult to detect anything by eye in a sea dominated by high-frequency wave fluctuations. Nonetheless its existence cannot be denied, and it is reasonable to assume that it is related to the discharge.

The ability to follow the feature over several hours yields further information. Figures 10b–d reveal that it moves gently with the tide, traveling a distance of about 400 m over three hours while compressing into a more compact region. If it were simply material floating on the surface, then we might expect tidal currents to have transported it rapidly beyond the field of view of the radar. Without additional observations from a boat, the only tentative conclusion to be drawn is that the feature revealed on the image is the first outcrop at the surface of a plume of water rising from the outfall. This would account for its movement with the tide, which is almost the behavior of a tethered object. The mechanism causing the enhanced backscatter is still to be determined.

b. Evolution of river plume front, Teignmouth

There is evidently considerable potential for using a coastal marine radar in conjunction with other measurements in experiments to study estuarine discharge and coastal water circulation. The radar enables the gradual evolution of such features to be monitored during a tidal cycle or over longer periods. An example of such a feature whose tidal behavior can be monitored with the radar is the river discharge front at Teignmouth in the English Channel.

Figure 11 displays a sequence of images revealing how the surface outcrop of the estuarine discharge front changes its shape and position as the tidal cycle develops. At 0922 UTC (Fig. 11a) it is just starting to emerge from the estuary. At 1000 (Fig. 11b) its southward edge can be seen spreading from the coast. By 1030 (Fig. 11c) the plume has ballooned into an almost circular shape about 1500 m in diameter and continues to expand (Fig. 11d). During this time the tidal currents were weak in the sea itself, which is why the plume remains almost symmetrical about the river mouth. There is corroborating evidence from simultaneous field measurements by the University of Plymouth, which confirms that this is indeed the surface signature of the front of the estuarine plume. Inside the widening arc of the front, the surface water flowing from inside the Teign estuary is fresher and less dense than the coastal water beyond. At the front the surface is rougher, producing the distinct bright line on the image, and in some parts of the plume this roughness appears to extend landward some distance from the front.

This case demonstrates another beneficial use of the radar, which was deployed in conjunction with the field experiment. The two research vessels engaged in measuring the plume evolution can be seen as point targets in the images. The radar operator was in radio communication with the research vessels and was able to

guide them to the exact location of the front which, although it appears clearly on this image, was not easily detected from a small vessel.

7. Discussion

The above examples demonstrate the variety of phenomena that can be observed by a shore-based marine radar using digital signal capture. They also indicate that there are a number of coastal oceanographic processes whose study can benefit from the deployment of such a radar. They clearly illustrate the utility of the marine radar as an oceanographic tool.

As with most methods of remote sensing, there are severe limitations to what can be achieved. Only surface phenomena, or those that have a surface signature, can be observed. The imaging mechanisms by which surface dynamic features are characterized by the backscatter are not very well understood for grazing incidence radar. The images it obtains generally have a poorer resolution and quality than the best satellite SAR images and they cover a smaller area. However, the importance of the method lies in its unique sampling capability. The image character of the data, covering two horizontal dimensions in considerable detail, makes it an excellent complement in coastal waters to in situ measurements of waves, fronts, temperature, etc., which are point measurements and limited in spatial coverage to linear transects or sparse arrays. The capacity to repeat the image measurements over exactly the same area, both at high frequency (25 times per min) and also regularly over hours and days, gives it a significant advantage over satellite SARs that can at best (given a number of satellites) revisit a site once a day. Thus, they can monitor the evolution of processes over timescales of minutes, hours, and a few days that is denied to satellite remote sensing methods. Even aircraft SARs, which can achieve a resampling period of about 20 min, are unable to collect the several images per minute, which enables high-frequency wave features on the image to be averaged out.

Consequently, there is potential for this measurement system to make a useful additional contribution to a diverse range of field experiments. As well as the obvious study of wave refraction, it can be used more widely in the study of beach processes, in the study of dispersal from piped outfalls, for the study of water movements, fronts and related water quality, and in studying the surface roughness processes of flow over bathymetric features. Given its robust nature and stationary deployment, the system can also play a long-term monitoring role. For example, it could be used to monitor the wave action on a beach between periods of intensive field measurements. It is worth noting that the system is capable of operating in all but the most extreme wind conditions and thus should return data during those storm events that may be both crucial for beach transport processes and hardest to monitor.

8. Conclusions

This paper has described a new way of applying the established technology of marine radars to the study of the coastal zone, by the simple expedient of locating the radar on the coast and capturing the data digitally at an 8-bit resolution. This approach has been reinforced by the development of a suite of processing software that enables the radar data to be presented as time sequences of geographically located images, capable of averaging and analysis in the time domain as well as the spatial. The applicability of this method to coastal oceanographic research has been demonstrated in a number of deployments. Some of the captured and processed images reveal phenomena as diverse as swell wave-crest patterns approaching the coast, evidence of pipe outfall plumes, estuarine fronts, and the location of breaker zones and flow over bathymetric features modulating surface roughness.

Our concern in this overview has been primarily to demonstrate the potential to use the approach to study a variety of processes. It is intended that a more detailed study of some of the phenomena discussed in this paper and a more complete analysis of the marine radar image data will be presented in subsequent publications.

Acknowledgments. The digital capture system was purchased with a special equipment grant provided by the Natural Environment Research Council. Some of the fieldwork costs were provided by the Commission of the European Communities (CEC) under International Scientific Cooperation Contract CI1-CT93-0061. MAT was supported by a grant from the Mexican Government. CPG was supported by a CEC Human Capital and Mobility Award ERBCHBICT930388. The authors are grateful for the technical support of Gary Fisher during deployments. The anonymous referees are thanked for their helpful suggestions for clarifying a number of points.

REFERENCES

Alpers, W., and I. Hennings, 1984: A theory of the imaging mechanism of underwater bottom topography by real and synthetic aperture radar. *J. Geophys Res.,* **89** (C), 10 529–10 546.

Buckley, J. R., M. Allingham, and R. Michaud, 1994: On the use of marine radar imagery for estimation of properties of the directional spectrum of the sea surface. *Atmos.–Ocean,* **32** (1), 195–213.

Chan, H. C., 1990: Radar sea clutter at low grazing angles. *IEEE Proc., Part F: Radar Signal Process.,* **137,** 102–112.

DeLoor, G. P., P. Hoogeboom, R. Spanhoff, and J. Bruisma, 1986: Microwave measurements over the North Sea. *Wave Dynamics and Radio Probing of the Ocean Surface,* O. M. Phillips and K. Hasselmann, Eds., Plenum Press, 505–516.

Gommenginger, C. P., N. P. Ward, G. J. Fisher, I. S. Robinson, and S. R. Boxall, 2000: Quantitative microwave backscatter measurements from the ocean surface using digital marine radar images. *J. Atmos. Oceanic Technol.,* **17,** 665–678.

Hirakuchi, H., and M. Ikeno, 1990: Wave direction measurement using marine X-band radar. *Proc. 22d Int. Conf. on Coastal Engineering,* Delft, Netherlands, Permanent International As-

sociation of Navigation Congresses and International Association for Hydraulic Research, 703–715.

Kerry, N. J., R. J. Burt, N. M. Lane, and M. T. Bagg, 1984: Simultaneous radar observations of surface slicks and in-situ measurements of internal waves. *J. Phys. Oceanogr.,* **14,** 1419–1423.

Lee, P. H. Y., and Coauthors, 1995: X-band microwave backscattering from ocean waves. *J. Geophys. Res.,* **100** (C2), 2591–2611.

Malinovsky, V. V., 1992: Evaluation of the relationship between parameters of the radar signal backscattered by the sea surface at grazing angles and the wind wave breaking characteristics. *Sov. J. Phys. Oceanogr.,* **3** (6), 443–454.

Scoon, A., and I. S. Robinson, 1993: SAR imaging of dynamical features in the English Channel. *Proc. First ERS-1 Symp.,* Cannes, France, European Space Agency, 119–124.

Seemann, J., F. Ziemer, and C. M. Senet, 1997: A method for computing calibrated ocean wave spectra from measurements with a nautical X-band radar. *Proc. Oceans '97,* Halifax, NS, Canada, MTS/IEEE, 1148–1154.

Tennyson, E. J., 1988: Shipboard navigational radar as an oil spill tracking tool. *Proc. 11th Arctic and Marine Oil Spill Program Technical Seminar,* Vancouver, BC, Canada, Environment Canada, 385–390.

Trask, J., M. Henschell, and B. Eid, 1994: Analysis of marine radar image spectra collected during the Grand Banks *ERS-1* SAR Wave Experiment. *Atmos.–Ocean,* **32** (1), 215–236.

Trizna, D. B., 1991: Statistics of low grazing angle radar sea clutter for moderate and fully developed ocean waves. *IEEE Trans. Antennas Propag.,* **39,** 1681–1690.

——, and D. Carlson, 1996: Studies of dual polarised low grazing angle radar sea scatter in nearshore regions. *IEEE Trans. Geosci. Remote Sens.,* **34,** 747–757.

——, J. P. Hansen, P. Hwang, and J. Wu, 1991: Laboratory studies of radar sea spikes at low grazing angles. *J. Geophys. Res.,* **96** (C7), 12 529–12 537.

Valenzuela, G. R., 1978: Theories for the interaction of electromagnetic and ocean waves—A review. *Bound.-Layer Meteor.,* **13,** 61–85.

Watson, G., and I. S. Robinson, 1990: A study of internal wave propagation in the Strait of Gibraltar using shore-based marine radar images. *J. Phys. Oceanogr.,* **20,** 374–395.

West J. C., J. M. Sturm, and M. Sletten, 1996: Small grazing angle radar scattering from a breaking water wave: Demonstration of Brewster angle damping. *Proc. IGARSS'96,* Lincoln, NE, IEEE Geoscience and Remote Sensing Society, 2207–2209.

Wetzel, L. B., 1990: Electromagnetic scattering from the sea at low grazing angles. *Surface Waves and Fluxes,* G. L. Geernaert and W. J. Plant, Eds., Vol. 2, *Remote Sensing,* Kluwer Academic, 146–171.

Williams, P. D. L., 1978: Applications of remote sensing by conventional radars. *Surveillance of Environmental Pollution and Resources by Electromagnetic Waves,* T. Lund, Ed., D. Reidel, 299–308.

Wright, J. W., 1968: A new model for sea clutter. *IEEE Trans. Antennas Propag.,* **16,** 217–223.